



CHORUS

This is the accepted manuscript made available via CHORUS. The article has been published as:

## Phonon Influence on Bulk Photovoltaic Effect in the Ferroelectric Semiconductor GeTe

Shi-Jing Gong, Fan Zheng, and Andrew M. Rappe

Phys. Rev. Lett. **121**, 017402 — Published 3 July 2018

DOI: [10.1103/PhysRevLett.121.017402](https://doi.org/10.1103/PhysRevLett.121.017402)

# Phonon influence on bulk photovoltaic effect in the ferroelectric semiconductor GeTe

Shi-Jing Gong<sup>1</sup>, Fan Zheng<sup>2</sup>, and Andrew M. Rappe<sup>2,\*</sup>

<sup>1</sup>*Key Laboratory of Polar Materials and Devices, Ministry of Education, Department of Electronic Engineering, East China Normal University, Shanghai 200062, China*

<sup>2</sup>*Department of Chemistry, University of Pennsylvania, Philadelphia, Pennsylvania 19104-6323, USA*

## Abstract

The shift current (SHC) has been accepted as the primary mechanism of the bulk photovoltaic effect (BPVE) in ferroelectrics, which is much different from the typical *p-n* junction-based photovoltaic mechanism in heterogeneous materials. In the present work, we use first-principles calculations to investigate the SHC response in the ferroelectric semiconductor GeTe, which is found possess a large SHC response due to its intrinsic narrow band gap and high covalency. We explore the changes of SHC response induced by phonon vibrations, and analytically fit current vs. vibrational amplitude to reveal the quantitative relationships between vibrations and SHC response. We discuss how modulation of the band gap and polarization reduces the SHC. Furthermore, we demonstrate the temperature dependence of the SHC response by averaging the phonon vibration influence in the Brillouin zone. Our investigation provides an explicit experimental prediction about the temperature dependence of BPVE, and can be extended to other classes of noncentrosymmetric materials.

## Introduction

The bulk photovoltaic effect (BPVE) refers to the generation of a steady photocurrent and above-band-gap photovoltage in a single-phase homogeneous material lacking inversion symmetry<sup>1-3</sup>. In the BPVE, a spontaneous direct short-circuit photocurrent is generated when electrons are continuously excited to quasiparticle coherent states that have intrinsic momentum, avoiding the need for an interface to separate the charge. Ferroelectric materials with spatial symmetry breaking are a primary focus of the BPVE research<sup>4-28</sup>. An early report related to BPVE demonstrated steady-state photovoltage and photocurrent in single-crystal BaTiO<sub>3</sub> in 1956<sup>1</sup>. Subsequently, this effect was further characterized in LiTaO<sub>3</sub><sup>2</sup>, LiNbO<sub>3</sub><sup>2,3</sup> and in SbS(I<sub>x</sub>Br<sub>1-x</sub>)<sup>29</sup>. More recently, BiFeO<sub>3</sub> has become the most popular single-phase multiferroic and has also attracted intense interest for its photovoltaic application. Large open-circuit photovoltages in BiFeO<sub>3</sub> films resulting from the BPVE have been experimentally observed<sup>15-17</sup>, and an increase in the power conversion efficiency of ferroelectric-based solar cells was reported<sup>16</sup>. As for the BPVE mechanism, models based on asymmetric scattering centers<sup>30</sup>, asymmetry in the electrostatic potential and the relativistic Rashba and Dresselhaus spin-orbit coupling<sup>31</sup> have been proposed. More recently, Young and Rappe<sup>32,33</sup> reformulated the shift current (SHC) theory<sup>34</sup>, enabling accurate BPVE predictions from first-principles calculations. This approach has been successfully applied to BiFeO<sub>3</sub><sup>32</sup>, BaTiO<sub>3</sub> (PbTiO<sub>3</sub>)<sup>33</sup>, and polar materials BiTeI<sup>35</sup> and CsPbI<sub>3</sub><sup>35</sup>, *etc.*, providing mechanistic insights and numerical results consistent with experimental measurements.

A wide variety of modified single-phase ferroelectric materials have been proposed in order to increase BPVE efficiency by reducing band gaps<sup>36-38</sup>. Alloys of PbTiO<sub>3</sub> doped with Ni<sup>2+</sup> were proposed<sup>39,40</sup>, leading to successful demonstration of Ni<sup>2+</sup> incorporation in (K, Ba)(Ni, Nb)O<sub>3-δ</sub> (KBNNO), the first report of a visible-light absorbing ferroelectric photovoltaic<sup>37</sup>. In 2015, Young *et al.* studied several ferroelectrics with the LiNbO<sub>3</sub> structure, *i.e.*, PbNiO<sub>3</sub>, Mg<sub>1/2</sub>Zn<sub>1/2</sub>PbO<sub>3</sub>, and LiBiO<sub>3</sub>,

which use electronegative  $B$  cations to raise the valence band, lowering the band gap and increasing the bulk photovoltaic response<sup>38</sup>. In addition, reducing band gap to enhance the SHC response has been theoretically reported in the nanolayered ferroelectric oxide system  $(\text{PbNiO}_2)_x(\text{PbTiO}_3)_{1-x}$ <sup>41</sup> and experimentally observed in ferroelectric complex oxide  $\text{Bi}_{3.25}\text{La}_{0.75}\text{Ti}_3\text{O}_{12}$  doped by Fe and Co<sup>42</sup>.

In order to enhance the SHC response both by lowering the band gap and by increasing the covalent bonding<sup>33</sup>, we turn our attention to polar semiconductors. In 2014, Brehm *et al.* theoretically examined the polar semiconductors  $\text{LiAsS}_2$ ,  $\text{LiAsSe}_2$ , and  $\text{NaAsSe}_2$ , and determined that they should offer forty times higher photocurrent than  $\text{BiFeO}_3$  under broad-band illumination<sup>43</sup>. In 2016, Tan *et al.* investigated the SHC response in the polar layered compounds  $\text{BiTeI}$  and  $\text{CsPbI}_3$ , which has a narrow and tunable band gap<sup>35</sup>. They obtained a large SHC response and found that the direction of BPVE can be reversed due to the band inversion at the topological phase transition induced by the strain<sup>35</sup>. In 2017, Rangel, Fregoso, and Cook, *et al.*, optimized the SHC theory and reported the large BPVE in single-layer monochalcogenides<sup>44-46</sup>. Recently, ferroelectric semiconductor  $\text{GeTe}$  has attracted renewed research attention due to its giant bulk Rashba spin-orbit coupling<sup>47,48</sup>, and it has become the prototype of a new class of multifunctional materials, *i.e.*, ferroelectric Rashba semiconductors<sup>49</sup>. With its dispersive  $sp$ -character conduction and valence bands, narrow band gap (0.6-0.7 eV), strong ferroelectric polarization (60-70  $\mu\text{C}/\text{cm}^2$ ), and high ferroelectric transition temperature (670 K-720 K)<sup>50, 51</sup>,  $\text{GeTe}$  could be a good candidate for photovoltaic devices with the BPVE. Furthermore, having only two atoms in the primitive unit cell,  $\text{GeTe}$  is undoubtedly the simplest ferroelectric, through which we can conveniently demonstrate the phonon influence on the SHC response, and help understand the temperature dependence of the BPVE in experiments.

## Computational Details

The plane-wave density functional theory (DFT) package

QUANTUM-ESPRESSO (QE) is used to perform the structural relaxations and electronic structure calculations, with the Perdew-Burke-Ernzerhof (PBE) generalized-gradient approximation (GGA) exchange-correlation functional<sup>52</sup>. All elements are represented by norm-conserving, optimized nonlocal pseudopotentials, with valence electrons of Ge and Te described by the configurations  $(4s^2 4p^2)$  and  $(5s^2 5p^4)$ <sup>53, 54</sup>, respectively. For the structural relaxation, self-consistent and non-self-consistent calculations, k-point grids of  $10 \times 10 \times 10$ ,  $14 \times 14 \times 14$  and  $54 \times 54 \times 54$  are used to ensure a well-converged SHC response. The phonon vibrational properties of GeTe are calculated using density-functional perturbation theory (DFPT)<sup>55</sup>, and the dynamical matrices are calculated based on the linear response. Spin-orbit coupling is included in all the calculations.

Our previously-developed approach, implemented in our in-house code, is used to calculate the SHC response. As was shown in Ref. [56], the SHC response is a second-order optical effect, which gives the current density:

$$J_q = \sigma_{rsq} E_r E_s$$

$$\begin{aligned} \sigma_{rsq}(\omega) = & \pi e \left( \frac{e}{m\hbar\omega} \right)^2 \sum_{n', n''} \int dk (f[n''\mathbf{k}] - f[n'\mathbf{k}]) \\ & \times \langle n'\mathbf{k} | \hat{P}_r | n''\mathbf{k} \rangle \langle n''\mathbf{k} | \hat{P}_s | n'\mathbf{k} \rangle \\ & \times \left( -\frac{\partial \phi_{n'n''}(\mathbf{k}, \mathbf{k})}{\partial k_q} - [\chi_{n''q}(\mathbf{k}) - \chi_{n'q}(\mathbf{k})] \right) \\ & \times \delta(\omega_{n''}(\mathbf{k}) - \omega_{n'}(\mathbf{k}) \pm \omega) \end{aligned}$$

where  $n'$  and  $n''$  index the bands,  $\mathbf{k}$  is the wave vector,  $\omega_n(\mathbf{k})$  is the energy of the  $n$ th band, and  $\sigma_{rsq}$  is a third-rank tensor giving current density  $\mathbf{J}$  as a response to the electromagnetic field  $\mathbf{E}$ . The expression is composed of a transition intensity multiplied by the so-called shift vector

$$R_q(n', n'', \mathbf{k}) = -\frac{\partial \phi_{n'n''}(\mathbf{k}, \mathbf{k})}{\partial k_q} - [\chi_{n''q}(\mathbf{k}) - \chi_{n'q}(\mathbf{k})],$$

where  $\chi_n$  is the Berry connection for band  $n$ , and  $\phi_{n'n''}$  is the phase of the momentum matrix element between bands  $n'$  and  $n''$ . The shift vector describes, on average, the displacement of coherent carriers during their lifetimes.

Ferroelectric GeTe belongs to the space group  $R3m$ , corresponding to the  $C_{3v}$  point group. With the rhombohedral lattice vectors in terms of Cartesian coordinates  $\vec{A}_1 = \left\{ \frac{a}{2}, -\frac{a}{2\sqrt{3}}, \frac{c}{3} \right\}$ ,  $\vec{A}_2 = \left\{ 0, -\frac{a}{\sqrt{3}}, \frac{c}{3} \right\}$ ,  $\vec{A}_3 = \left\{ -\frac{a}{2}, -\frac{a}{2\sqrt{3}}, \frac{c}{3} \right\}$ , the ferroelectric polarization is along the z direction, and the shift current response tensor has the form,

$$\sigma = \begin{bmatrix} 0 & 0 & 0 & 0 & \sigma_{yz}Y & -\sigma_{yy}Y \\ -\sigma_{yy}Y & \sigma_{yy}Y & 0 & \sigma_{yz}Y & 0 & 0 \\ \sigma_{xx}Z & \sigma_{xx}Z & \sigma_{zz}Z & 0 & 0 & 0 \end{bmatrix}$$

## Results and discussion

Shown in Fig. 1(a) are the primitive unit cell and the first Brillouin zone of distorted GeTe, with the ferroelectric polarization along the  $z$  direction. The lattice parameter  $a$ , the angle  $\alpha$ , and the high symmetry k-points  $\Gamma$ ,  $Z$ ,  $L$ , and  $U$  are indicated. The relative shift of the Ge and Te sublattices is reported using the distorted rocksalt setting: atomic positions are  $(0, 0, 0)$  and  $(0.5-\tau, 0.5-\tau, 0.5-\tau)$  for Ge and Te, respectively. The relaxed structure has lattice constant  $a \sim 4.41 \text{ \AA}$ , the angle  $\alpha \sim 58.08^\circ$ , and the ferroelectric deviation  $\tau \sim 0.0285$ , and the ferroelectric polarization is  $60 \text{ \mu C/cm}^2$ , consistent with previous reports about GeTe.<sup>57-60</sup> The indirect band gap is  $0.70 \text{ eV}$ , with valence-band maximum at the  $Z$  point and conduction-band minimum at the  $L$  point, a little larger than the experimental value ( $0.61 \text{ eV}$ )<sup>50, 51</sup>. Along the  $\Gamma$ - $Z$  line, the inversion-symmetry-breaking potential and the wave vector  $k$  are parallel, so no Rashba spin splitting is observed, while along the line  $Z$ - $U$ , which is perpendicular to the ferroelectric field, a large Rashba spin splitting is obtained, as has been reported by Sante *et al.*<sup>47</sup>

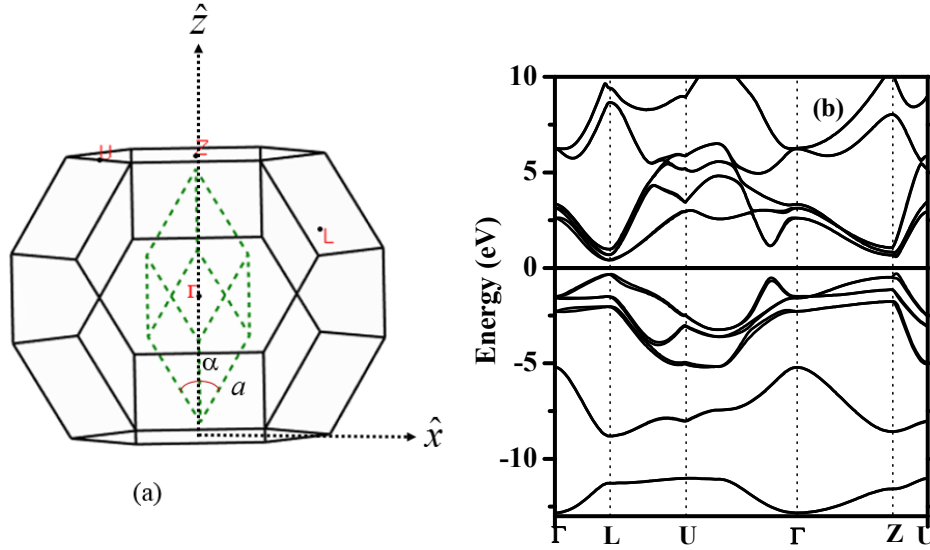


Fig. 1 (a) The rhombohedral unit-cell of GeTe (green dotted lines) and the first Brillouin zone (black solid lines), with the ferroelectric polarization along the  $\hat{z}$  direction. (b) The band structure of ferroelectric GeTe, with the conduction-band minimum at the L point and valence-band maximum at the Z point.

Based on the relaxed structure, we calculate the phonon vibrations at the  $\Gamma$  point. No imaginary phonon modes are found, confirming the stability of the ferroelectric structure. The primitive unit cell of GeTe contains two atoms, which gives rise to six phonon vibration modes. The three modes of zero frequency at the  $\Gamma$  point are the translational modes, for which both Ge and Te atoms move with the same displacement. These translational modes have no influence on the SHC response. For each of the three optic modes, Ge and Te atoms vibrate along the same axis but with opposite direction. Since both the  $x$ - and  $y$ -axis vibrations are perpendicular to the ferroelectric polarization, and they have the same influence on the SHC response, we only show the phonon mode along the  $x$ -axis in Fig. 2(a). In Fig. 2(b), we show the phonon vibration parallel to the ferroelectric polarization, and refer to it as “ferroelectric vibration”. For a nonzero phonon momentum, there is a phase difference between the atomic displacements in the different unit cells. Therefore, a supercell is required to accommodate all atoms vibrating with different phases to retain the periodicity. For the phonons at  $Z(0.5, 0.5, 0.5)$ , we use a  $2 \times 2 \times 2$  supercell to

include the  $\pi$  phase. In particular, we consider the vibrational mode that has all the atoms moving along the ferroelectric direction; however, in one unit cell, the ferroelectric polarization is enhanced by the vibration, and in its counterpart unit, the ferroelectric polarization is decreased, as shown in Fig. 2(c). Compared with the ferroelectric vibration at the  $\Gamma$  point, this phonon vibration at the  $Z$ -point is called “*antiferroelectric-like mode*”.

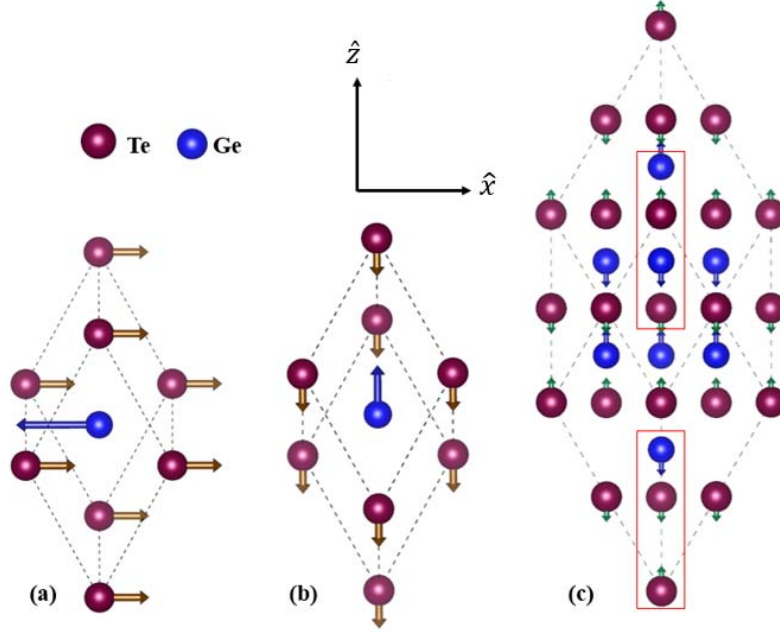


Fig. 2 Three kinds of phonon vibrations: the phonon vibration along the (a)  $\hat{x}$  and (b)  $\hat{z}$  direction in the primitive unit cell, and (c) the *antiferroelectric-like* vibration mode in the  $2 \times 2 \times 2$  supercell.

To evaluate the phonon vibrational amplitude, we use the formula  $\frac{1}{2} \sum_i m_i v^2 (\lambda u_i^{x,y,z})^2 = \frac{1}{2} k_B T$ , in which  $k_B$  is the Boltzmann constant,  $T$  is the temperature,  $v$  is phonon vibration frequency,  $m_i$  is the mass of the  $i$ th atom in the unit cell,  $\lambda$  is defined as the phonon vibration amplitude,  $u_i^{x,y,z}$  is the unified unitless phonon eigenvector component with  $\sum_i |u_i^{x,y,z}|^2 = 1$ , and  $\lambda u_i^{x,y,z}$  indicates the  $x$ ,  $y$  and  $z$  direction vibration displacement of the  $i$ th atom. It is clear that the higher the vibration frequency is, the smaller the vibrational amplitude is. At the room

temperature ( $T=300$  K), we get the vibrational amplitude  $\lambda \sim 0.07$  Å for the ferroelectric vibration mode ( $\nu=127$  cm<sup>-1</sup>),  $\lambda \sim 0.1$  Å for the perpendicular vibration mode ( $\nu=83$  cm<sup>-1</sup>), and  $\lambda \sim 0.03$  Å for the antiferroelectric vibration mode ( $\nu=172$  cm<sup>-1</sup>). The phonon frequencies are consistent with the previous report .

Taking the phonon vibration into account, the SHC response can be described in terms of vibrational amplitude  $\lambda$ :  $C(\omega, \lambda) = C_0(\omega) + C_1(\omega)\lambda + C_2(\omega)\lambda^2 + C_4(\omega)\lambda^4 + \mathcal{O}(\lambda^6)$ , where  $\omega$  is the photon frequency and  $C_0(\omega)$  indicates the SHC response without phonon vibration. For the ferroelectric vibration, the linear term  $C_1(\omega)\lambda$  dominates for small vibrational amplitudes, and the nonlinear effect becomes important for relatively large vibrational amplitudes. For the perpendicular vibration, the linear term  $C_1(\omega)$  is zero, and only even terms survive. For the general vibration which includes both  $x/y$  and  $z$  movement, both the linear and nonlinear items should be included.

The calculated SHC coefficient  $\sigma_{zzz}$  under different ferroelectric vibration amplitudes is shown in Fig. 3(a), in which positive/negative amplitudes mean that the ferroelectric displacement is decreased/increased by the phonon vibration. Without the phonon vibration ( $\lambda=0$  in Fig. 3(a)), we find that the  $\sigma_{zzz}$  coefficient of GeTe is about five times larger than that of BiFeO<sub>3</sub> ( $\sim 3.5 \times 10^{-4}$  A/W)<sup>32</sup>. It is known that the ferroelectric polarization of BiFeO<sub>3</sub> is about 90  $\mu\text{C}/\text{cm}^2$ , and the fundamental band gap is about 2.58 eV<sup>32</sup>. Although the polarization of GeTe is smaller than that of BiFeO<sub>3</sub>, its SHC response is larger, suggesting that the narrow band gap and the covalency play more critical roles than the precise polarization magnitude. The SHC response of bulk GeTe has a broad peak around the energy range 0.9-1.2 eV, and thus

significant BPVE can be excited by visible and near-IR light. In addition, we note that while increasing (decreasing) the ferroelectric displacement does increase (decrease) the SHC response, the change of the SHC response is not linearly dependent on the change of the ferroelectric displacement. However, the evolution of the band structure with the ferroelectric phonon vibrations links increasing (decreasing) the ferroelectric displacement with decrease (increase) of the band gap. The direct effect of the soft-mode phonon on SHC and its indirect effect via band-gap change have opposite contributions to the SHC response and will surely result in a nonlinear relationship between the integrated SHC response change and the ferroelectric vibration amplitude.

To further investigate the asymmetrical SHC change induced by the positive and negative ferroelectric vibration, we select the photon energies of 0.9 eV and 1.1 eV, and plot the change of the SHC response versus the vibration amplitude in Fig. 3(b). The solid triangles and squares indicate the results from the first-principles calculations, and the lines represent the fitting from the polynomial  $C_1(\omega)\lambda + C_2(\omega)\lambda^2$ . For  $\hbar\omega = 0.9$  eV, we get  $C_1(\omega) = 0.006$  A/ÅW,  $C_2(\omega) = -0.012$  A/Å<sup>2</sup>W, and for  $\hbar\omega = 1.1$  eV, we get  $C_1(\omega) = 0.008$  A/ÅW,  $C_2(\omega) = -0.040$  A/Å<sup>2</sup>W. We can see that for different photon energies, the parameters  $C_1(\omega)$  and  $C_2(\omega)$  are quite different, and the polynomial with both the first and second order of the vibrational amplitude can well fit the first-principles SHC calculations. If we continue to increase the vibration amplitude, higher orders must be considered.

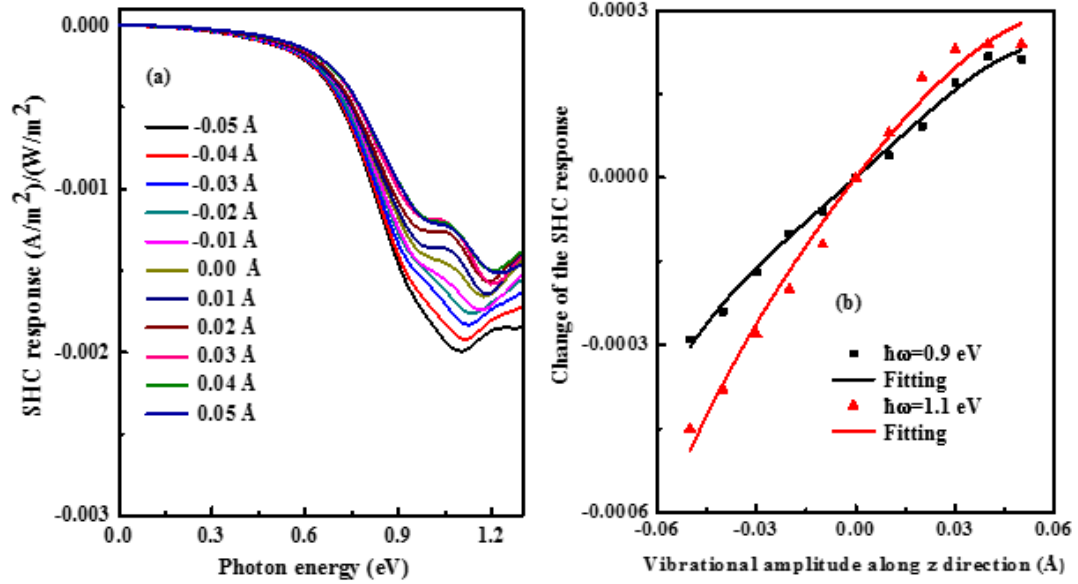


Fig. 3 (a) The shift current response ( $\sigma_{zz}$ ) of GeTe versus photon energy, and its dependence on the ferroelectric vibrational amplitude. (b) The change of the shift current response versus the vibrational amplitude, with the photon energy  $\hbar\omega=0.9$  eV and 1.1 eV, respectively. The squares and triangles in (b) are the results from the first-principles calculations, and the lines in black and red are the fitting curves from the polynomial  $C_1(\omega)\lambda+C_2(\omega)\lambda^2$ .

We next investigate the influence of the perpendicular phonon vibrations (see Fig. 4(a)) on the SHC response. As the vibrational amplitude is increased from zero to  $0.10 \text{ \AA}$ , we observe a gradual decrease of the SHC response. Compared with the ferroelectric vibration shown in Fig. 3, we notice that this vibration mode can decrease the SHC response more significantly, since the vibrations decrease the ferroelectric polarization and increase the band gap, both of which help to decrease the SHC response. Since the positive and negative vibrations make no difference for the SHC response, the relation between the change of the SHC and the vibration

amplitudes should be described by a polynomial only with the even orders of the vibration amplitude. In Fig. 4(b), we plot the dependence of the SHC on the vibrational amplitude. We select the photon energies  $\hbar\omega=1.0, 1.2$  eV, and use the polynomial  $C_2(\omega)\lambda^2$  to fit the first-principles calculations. It can be clearly seen that the first-principles results can be well fitted by the parabolic formula. For  $\hbar\omega=1.0$  eV, we find the  $C_2(\omega)=0.71$  A/Å<sup>2</sup>W, and for  $\hbar\omega=1.2$  eV,  $C_2(\omega)=0.90$  A/Å<sup>2</sup>W.

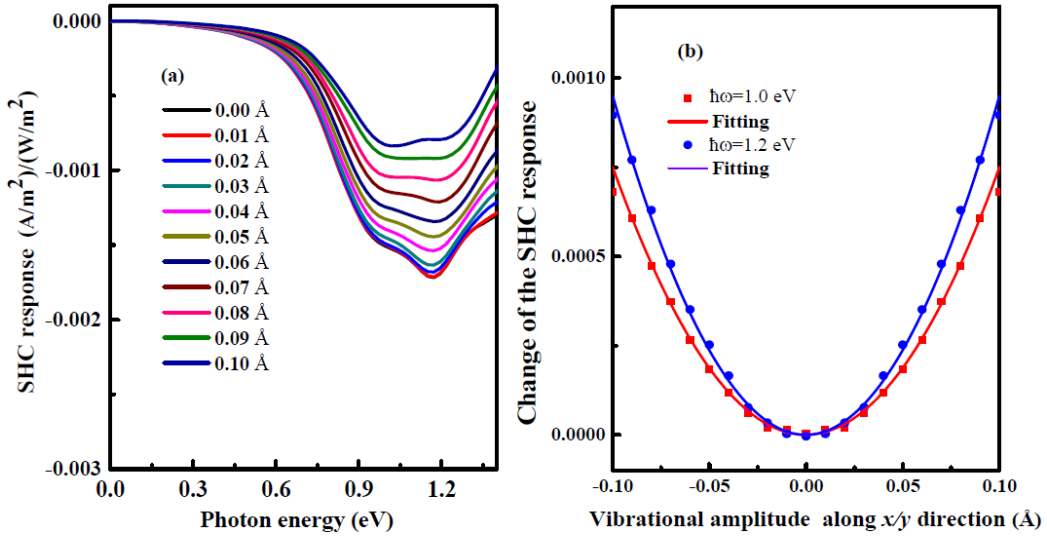


Fig. 4 (a) The shift current response ( $\sigma_{zzz}$ ) versus the photon energy, and its dependence on the perpendicular phonon vibrational amplitude. (b) The change of the shift current response versus the amplitude  $\lambda$ , with the photon energy  $\hbar\omega=1.0$  eV and 1.2 eV, respectively. The squares and triangles in (b) are the results from the first principles calculations, and the lines in black and red are the fitting curves from the polynomial  $C_2(\omega)\lambda^2$ .

We then explore the phonon vibration at the nonzero phonon momentum. For the phonon momentum  $Z(0.5, 0.5, 0.5)$ , we consider a  $2\times 2\times 2$  supercell, focusing on the *antiferroelectric*-like vibration at the Z point (see Fig. 2(c)). Intuitively, this kind of phonon vibration ought not have influence on SHC response, due to the opposing vibrations induced by the  $\pi$  phase difference. We computationally consider the vibration amplitude less than 0.03 Å. Due to the  $\pi$  phase, positive and negative phonon amplitudes will have the same effect on the SHC, which is different from the ferroelectric vibration mode at the  $\Gamma$  point. We therefore use the same polynomial

$C_2(\omega)\lambda^2$  that is applicable to the perpendicular vibration at the  $\Gamma$  point. Another interesting point is that we find that this kind of phonon vibration can increase the SHC response. As can be clearly seen in Fig. 5(a), the absolute value of the SHC response increases with increasing vibration amplitude, especially for photon energy  $\hbar\omega$  within 0.9-1.2 eV. The change of the SHC response can be well fitted by the parabola  $C_2(\omega)\lambda^2$  with  $C_2(\omega)=-0.08 \text{ A}/\text{\AA}^2\text{W}$  for  $\hbar\omega=0.9 \text{ eV}$  and  $C_2(\omega)=-0.3 \text{ A}/\text{\AA}^2\text{W}$  for  $\hbar\omega=1.1 \text{ eV}$ , as shown in Fig. 5(b). Since both  $C_0(\omega)$  and  $C_2(\omega)$  are negative, the SHC response can be increased by this *antiferroelectric-like* vibration mode.

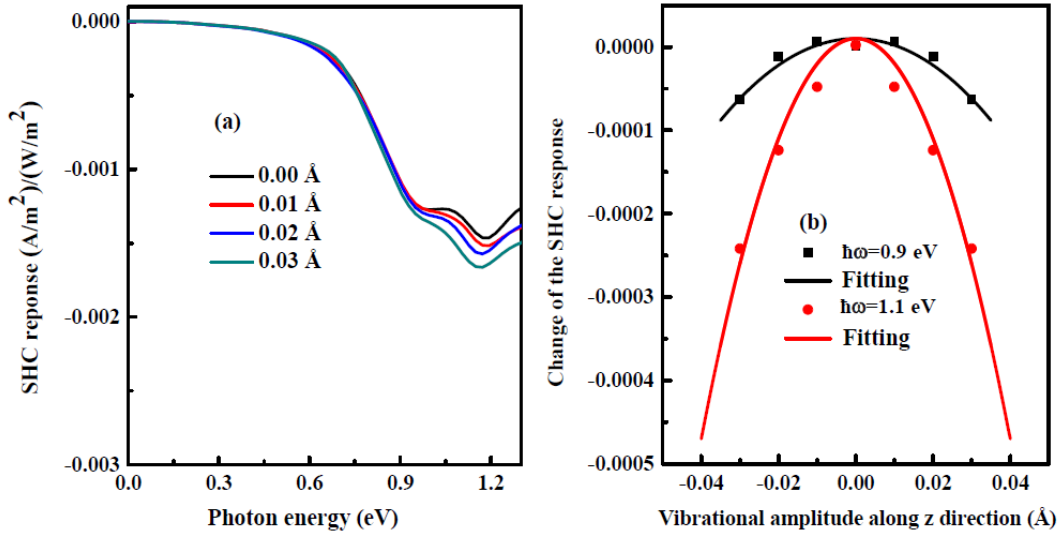


Fig. 5 (a) The shift current response ( $\sigma_{zz}$ ) versus the photon energy, and its dependence on the *antiferroelectric-like* phonon vibrational amplitude. (b) The change of the shift current response versus the amplitude  $\lambda$ , with the photon energy  $\hbar\omega=0.9 \text{ eV}$  and  $1.1 \text{ eV}$ , respectively. The squares and circles in (b) are the results from the first-principles calculations, and the lines in black and red are the fitting curves from the parabola  $C_2(\omega)\lambda^2$ .

From the above analysis, we know that different phonon vibration modes have different contributions to the SHC response. However, to make explicit predictions of experiments, we sample the phonon Brillouin zone with a uniform  $q$ -grid, and obtain the  $q$ -averaged SHC response. We consider a  $2\times 2\times 2$   $q$ -grid, based on which 48 vibration modes are included. These modes include the  $x/y/z$ -direction vibrations discussed above, and mixed direction vibrations. For each vibrational mode, we

consider the temperature range from 0 K to 300 K. To relieve the computational burden, we somewhat decrease the stringency of the calculation criteria and check the convergence of the shift-current response. We use the equipartition theorem in terms of the temperature effect, *i.e.* each phonon mode will acquire energy of  $\frac{1}{2}k_B T$ . In Figs. 6 (a) and (b), we show the SHC response ( $\sigma_{zzz}$ ) versus the photon energy and temperature, respectively. It is clear that the SHC response gradually decreases with increasing temperature. The temperature effect is more obvious for photon energies around 1.0 eV, which is consistent with the single vibration modes discussed above. If we extend the temperature to the Curie temperature, the shift-current response will decrease to zero due to the loss of ferroelectric polarization and the restoration of centrosymmetry.

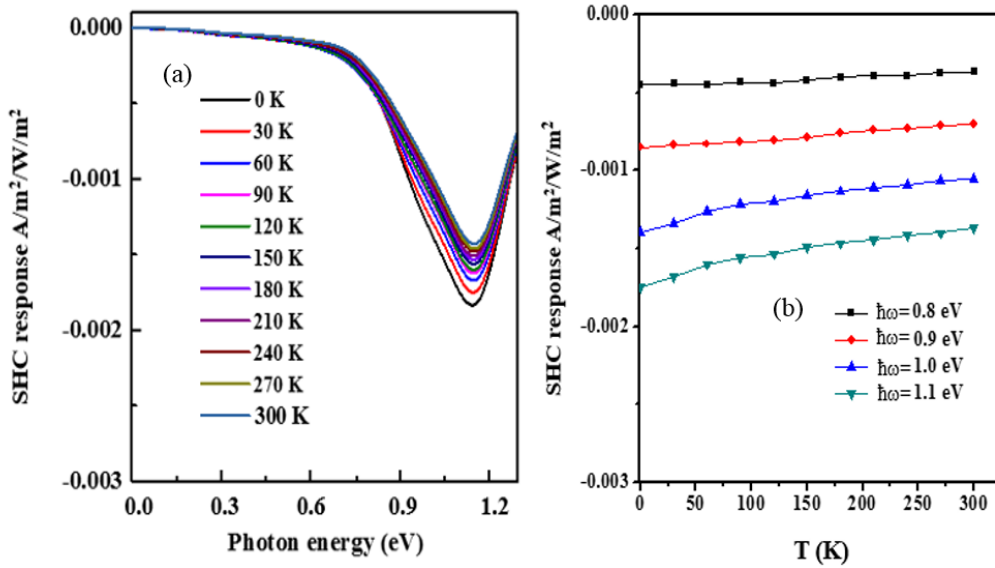


Fig. 6 (a) The shift current response ( $\sigma_{zzz}$ ) versus the photon energy for different temperatures. (b) Temperature dependence of the shift current response ( $\sigma_{zzz}$ ) with the photon energy  $\hbar\omega=0.8, 0.9, 1.0, 1.1$  eV.

In summary, we investigate the SHC response in the bulk GeTe, which has been identified as a prototypical compound of a new class of multifunctional materials, *i.e.*, ferroelectric Rashba semiconductors. It is found that the SHC response in GeTe is about five times larger than that of BiFeO<sub>3</sub>, whose strong ferroelectricity favors the large SHC response while the relatively large band gap suppresses it. Through the

representative phonon vibration modes, including phonon vibrations at the  $\Gamma$  point, and the *antiferroelectric*-like phonon vibration at the finite phonon wavevectors, we explore the phonon influence on the SHC response. By using analytic fits, we reveal the quantitative relationships between vibrational amplitudes and the SHC response. Furthermore, we explicitly present the experimental prediction about the temperature dependence of the SHC response by averaging the phonon vibration influence in the Brillouin zone. Our investigation can help understand the temperature dependence of the BPVE in experiments, and can be extended to other classes of noncentrosymmetric materials.

### Acknowledgement

This work was supported by a grant from the US Department of Energy, Office of Basic Energy Sciences, under grant DE-FG02-07ER46431, NSFC with grant No. 61774059 and NSFS with grant No.18ZR1412500. Computational support was provided by the NERSC of the DOE.

Corresponding author: rappe@sas.upenn.edu

- <sup>1</sup> A. G. Chynoweth, Phys. Rev. **102**, 705 (1956).
- <sup>2</sup> F. S. Chen, J. Appl. Phys. **40**, 3389 (1969).
- <sup>3</sup> A. M. Glass, D. von der Linde, and T. J. Negran, Appl. Phys. Lett. **25**, 233 (1974).
- <sup>4</sup> S. Y. Yang, et al., Nat. Nanotech. **5**, 143 (2010).
- <sup>5</sup> G. Chanussot, V. M. Fridkin, G. Godefroy, and B. Jannot, Appl. Phys. Lett. **31**, 3 (1977).
- <sup>6</sup> V. M. Fridkin, Crystallogr. Rep. **46**, 654 (2001).
- <sup>7</sup> L. Z. Tan, F. Zheng, S. M. Young, F. Wang, S. Liu, and A. M. Rappe, npj Comput. Mater. **2**, 16026 (2016).
- <sup>8</sup> J. Seidel, D. Fu, S.-Y. Yang, E. Alarcón-Lladó, J. Wu, R. Ramesh, and J. W. Ager, Phys. Rev. Lett. **107**, 126805 (2011).
- <sup>9</sup> L. Chen, Q. Lin, J. Hart, S. Li, and D. Wang, Int. J. Appl. Ceram. Technol. **13**, 896 (2016).
- <sup>10</sup> P. Lopez-Varo, et al., Phys. Rep. **653**, 1 (2016).
- <sup>11</sup> A. Pérez-Tomás, M. Lira-Cantú, and G. Catalan, Adv. Mater. **28**, 9644 (2016).
- <sup>12</sup> A. Zenkevich, Y. Matveyev, K. Maksimova, R. Gaynutdinov, A. Tolstikhina, and V. Fridkin, Phys. Rev. B **90**, 161409 (2014).
- <sup>13</sup> H. Wang, G. Gou, and J. Li, Nano Energy **22**, 507 (2016).
- <sup>14</sup> D. J. Kim and M. Alexe, Appl. Phys. Lett. **110**, 183902 (2017).

15 A. Bhatnagar, A. Roy Chaudhuri, Y. Heon Kim, D. Hesse, and M. Alexe, *Nat. Commun.* **4**, 2835  
(2013).

16 M. Alexe and D. Hesse, *Nat. Commun.* **2**, 256 (2011).

17 T. Choi, S. Lee, Y. J. Choi, V. Kiryukhin, and S.-W. Cheong, *Science* **324**, 63 (2009).

18 C. Somma, K. Reimann, C. Flytzanis, T. Elsaesser, and M. Woerner, *Phys. Rev. Lett.* **112**, 146602  
(2014).

19 W. T. H. Koch, R. Munser, W. Ruppel, and P. Würfel, *Solid State Commun.* **17**, 847 (1975).

20 M. Nakamura, F. Kagawa, T. Tanigaki, H. S. Park, T. Matsuda, D. Shindo, Y. Tokura, and M.  
Kawasaki, *Phys. Rev. Lett.* **116**, 156801 (2016).

21 L. Pintilie, V. Stancu, E. Vasile, and I. Pintilie, *J. Appl. Phys.* **107**, 114111 (2010).

22 W. Ji, K. Yao, and Y. C. Liang, *Phys. Rev. B* **84**, 094115 (2011).

23 N. Seiji, U. Tomohisa, N. Daichi, F. Hironori, K. Masafumi, and S. Masaru, *Jpn. J. Appl. Phys.* **53**,  
09PA16 (2014).

24 K. Nonaka, M. Akiyama, T. Hagi, and A. Takase, *Jpn. J. Appl. Phys.* **34**, 2344 (1995).

25 D. Daranciang, et al., *Phys. Rev. Lett.* **108**, 087601 (2012).

26 K. T. Butler, J. M. Frost, and A. Walsh, *Energy Environ. Sci.* **8**, 838 (2015).

27 J. E. Spanier, et al., *Nat. Photonics* **10**, 611 (2016).

28 R. Nechache, C. Harnagea, S. Li, L. Cardenas, W. Huang, J. Chakrabartty, and F. Rosei, *Nat.*  
*Photonics* **9**, 61 (2014).

29 A. A. Grekov, M. A. Malitskaya, V. D. Spitsina, V. M. Fridkin, *Kristallografiya* **15**, 500 (1970)

30 V. I. Belinicher, B. I. Sturman, *Sov. Phys. Usp.* **23**, 199 (1980).

31 G. Dresselhaus, *Phys. Rev.* **100**, 580 (1955).

32 S. M. Young, F. Zheng, and A. M. Rappe, *Phys. Rev. Lett.* **109**, 236601 (2012).

33 S. M. Young and A. M. Rappe, *Phys. Rev. Lett.* **109**, 116601 (2012).

34 R. von Baltz and W. Kraut, *Phys. Rev. B* **23**, 5590 (1981).

35 L. Z. Tan and A. M. Rappe, *Phys. Rev. Lett.* **116**, 237402 (2016).

36 F. Wang and A. M. Rappe, *Phys. Rev. B* **91**, 165124 (2015).

37 I. Grinberg, et al., *Nature* **503**, 509 (2013).

38 S. M. Young, F. Zheng, and A. M. Rappe, *Phys. Rev. Appl.* **4**, 054004 (2015).

39 G. Y. Gou, J. W. Bennett, H. Takenaka, and A. M. Rappe, *Phys. Rev. B* **83**, 205115 (2011).

40 J. W. Bennett, I. Grinberg, and A. M. Rappe, *J. Am. Chem. Soc.* **130**, 17409 (2008).

41 F. Wang, S. M. Young, F. Zheng, I. Grinberg, and A. M. Rappe, *Nat. Commun.* **7**, 10419 (2016).

42 H. An, J. Y. Han, B. Kim, J. Song, S. Y. Jeong, C. Franchini, C. W. Bark, and S. Lee, *Sci. Rep.* **6**,  
28313 (2016).

43 J. A. Brehm, S. M. Young, F. Zheng, and A. M. Rappe, *J. Chem. Phys.* **141**, 204704 (2014).

44 T. Rangel, B. M. Fregoso, B. S. Mendoza, T. Morimoto, J. E. Moore, and J. B. Neaton, *Phys. Rev.*  
*Lett.* **119**, 067402 (2017).

45 B. M. Fregoso, T. Morimoto, and J. E. Moore, *Phys. Rev. B* **96**, 075421 (2017).

46 A. M. Cook, B. M. Fregoso, F. de Juan, S. Coh, and J. E. Moore, *Nat. Commun.* **8**, 14176 (2017).

47 D. Di Sante, P. Barone, R. Bertacco, and S. Picozzi, *Adv. Mater.* **25**, 509 (2013).

48 H. J. Elmers, et al., *Phys. Rev. B* **94**, 201403 (2016).

49 S. Picozzi, *Front. Physics* **2**, 10 (2014).

50 J.-W. Park, S. H. Eom, H. Lee, J. L. F. Da Silva, Y.-S. Kang, T.-Y. Lee, and Y. H. Khang, *Phys. Rev. B*  
**80**, 115209 (2009).

- 51 J.-W. Park, et al., Appl. Phys. Lett. **93**, 021914 (2008).
- 52 P. Giannozzi, et al., J. Phys.: Condens. Matter **21**, 395502 (2009).
- 53 A. M. Rappe, K. M. Rabe, E. Kaxiras, and J. D. Joannopoulos, Phys. Rev. B **41**, 1227 (1990).
- 54 N. J. Ramer and A. M. Rappe, Phys. Rev. B **59**, 12471 (1999).
- 55 S. Baroni, S. de Gironcoli, A. Dal Corso, and P. Giannozzi, Rev. Mod. Phys. **73**, 515 (2001).
- 56 J. E. Sipe and A. I. Shkrebtii, Phys. Rev. B **61**, 5337 (2000).
- 57 U. D. Wdowik, K. Parlinski, S. Rols, and T. Chatterji, Phys. Rev. B **89**, 224306 (2014).
- 58 R. Shaltaf, E. Durgun, J. Y. Raty, P. Ghosez, and X. Gonze, Phys. Rev. B **78**, 205203 (2008).
- 59 M. J. Polking, et al., Nat. Mater. **11**, 700 (2012).
- 60 A. Ciucivara, B. R. Sahu, and L. Kleinman, Phys. Rev. B **73**, 214105 (2006).